HHS Public Access

Author manuscript

J Thorac Cardiovasc Surg. Author manuscript; available in PMC 2023 December 01.

Published in final edited form as:

J Thorac Cardiovasc Surg. 2022 December ; 164(6): e371–e384. doi:10.1016/j.jtcvs.2021.07.062.

Extracellular Vesicles Improve Diastolic Function and Substructure in Normal and High Fat Diet Models of Chronic Myocardial Ischemia

Ahmed Aboulgheit, MD[1,2], **Catherine Karbasiafshar, BS**[1], **Mohamed Sabra, MD**[1], **Zhiqi Zhang, MD**[1,2], **Neel Sodha, MD**[2], **M. Ruhul Abid, MD PhD**[1,2], **Frank W. Sellke, MD**[1,2]

[1]Cardiovascular Research Center, Rhode Island Hospital, Providence RI 02903.

[2]Division of Cardiothoracic Surgery, Alpert Medical School of Brown University and Rhode Island Hospital, Providence, RI 02903

Abstract

Objective: The burden of mortality and morbidity of cardiovascular disease is in part attributed to substantial fibrosis accelerated by coexisting risk factors. This study aims to evaluate the effect of extracellular vesicle therapy on diastolic function and myocardial fibrosis in the setting of chronic myocardial ischemia with and without high fat diet.

Methods: Forty male Yorkshire swine were administered a normal or high fat diet. At eleven weeks of age, they underwent placement of an ameroid constrictor on their left circumflex coronary artery. Both dietary groups then received either intramyocardial injection of vehicle saline as controls (C) or extracellular vesicles as treatment (EVs) into the ischemic territory (ND-C, n=8, HFD-C, n= 11) or EVs; (ND-EV n=9, HFD-EV n= 12). Five weeks later hemodynamic parameters, histology, and selected protein expression were evaluated.

Results: Extracellular vesicles reduced end diastolic pressure volume relationship (p=0.002), perivascular collagen density (p=0.031), calcium mineralization (p=0.026), and cardiomyocyte diameter (p<0.0001); and upregulated osteopontin (p=0.0046) and mechanistic target of rapamycin (p=0.021). Interaction between extracellular vesicles and diet were observed in vimentin area (p=0.044) and fraction of myofibroblast markers to total vimentin (p=0.049). Significant changes across diet were found with reductions in muscle fiber area (p=0.026), tumor necrosis factor α (p= 0.0002), NADPH oxidase 2 and 4 (p=0.0036, p=0.008), superoxide dismutase 1 (p=0.034), and phosphorylated glycogen synthase kinase 3β (p=0.020).

Corresponding Author: Frank W. Sellke MD, Karlson and Karlson Professor of Surgery and Chief of Cardiothoracic Surgery, Warren Alpert Medical School at Brown University and Rhode, Island Hospital, MOC 360, 2 Dudley Street, Providence, RI, 02905; fsellke@lifespan.org; (401) 444-2732.

Conflict of Interest Statement: The authors report no conflicts of interest.

AATS Meeting Presentation

Conclusion: Extracellular vesicle therapy improved the myocardium's ability to relax, and is likely attributed to structural improvements at the extracellular matrix and cellular levels.

Central Picture

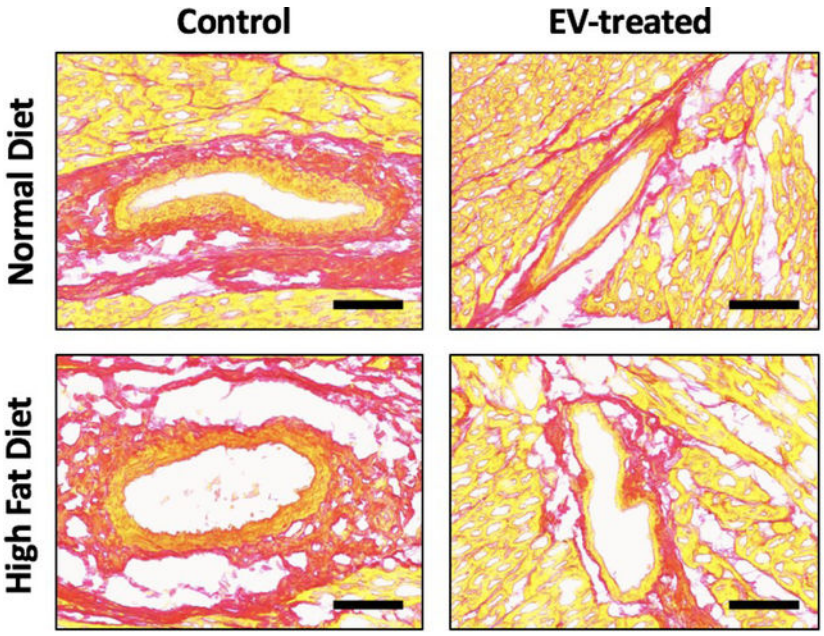

Central Picture Legend

EVs reduced perivascular fibrosis in swine with chronic myocardial ischemia.

Central Message

Extracellular vesicle therapy improved the myocardium's ability to relax across both normal and high fat diet models of chronic myocardial ischemia.

Graphical Abstract

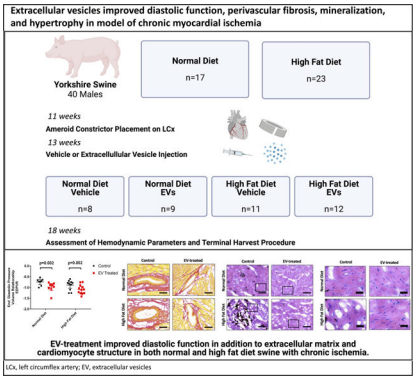

A schematic of the methods outlines the experimental design beginning with the administration of a normal or high fat diet, followed by induction of chronic myocardial ischemia, then extracellular vesicle treatment. Five weeks post-control or treatment, animals were assessed for hemodynamic parameters and tissue was collected. Findings include significant improvement in

End Diastolic Pressure Volume Relationship (EDPVR), accompanied by improvements in the myocardial substructure, with reduced perivascular fibrosis, mineralization, and cardiomyocyte hypertrophy. LCx, left circumflex artery; EV, extracellular vesicles.

Keywords

Extracellular Vesicles; Cardiovascular Disease; Metabolic Stress; Fibrosis

Introduction

Ischemic heart disease continues to be the leading cause of death worldwide and contributes to significant morbidity in patients with refractory disease not amenable to revascularization.[1] Chronic persistence of the ischemic insult leads to irreversible injury and loss of functional cardiomyocytes, which are permanent cells incapable of regeneration. Therefore, healing occurs by formation of stiff, non-contractile scar tissue which is the hallmark of myocardial fibrosis. Perpetuation of tissue injury and inflammation lead to recruitment of resident fibroblasts and transition to a mesenchymal secretory fibroblast phenotype that contribute to reparative and reactive fibrosis. Reparative fibrosis is characterized by patchy interstitial collagen deposition secondary to cardiomyocyte death in the setting of pronounced inflammation, whereas reactive fibrosis features accumulation of fibrous tissue in perivascular regions surrounding coronary arteries and tends to occur in chronic disease states such as hypertension, metabolic syndrome, and ischemia.[2]

Abundance of type I collagen seen in the perivascular type is associated with increased stiffness and diastolic dysfunction, seen with hypertension and aortic stenosis, and also characterized by cardiac hypertrophy.[3] On the other hand, the myocardium in systolic or forward failure typically exhibits realignment of collagen, loss of cardiomyocytes, and left ventricular dilation.[3] Hypertension, dyslipidemia and diabetes are among prevalent risk factors associated with the progression of fibrotic remodeling that gives rise to diastolic dysfunction,[4] Eventually, the significant restriction in myocardial filling impedes adequate venous return whereas contractility remains relatively unaffected. Once the degree of fibrosis exceeds systemic and/or pulmonary venous capacitance, heart failure with preserved ejection fraction (HFpEF) occurs, which is prevalent in about 30% of the general population.[5] Pharmacological management of HFpEF is mainly aimed at decreasing cardiac preload thus ameliorating symptoms of congestion or augmenting contractility when systolic compromise occurs. To date, no curative treatment is known to effectively reverse or halt the progression of the inciting pathology.[6]

The field of extracellular vesicles (EVs) has emerged as a prospective therapeutic approach following the lack of success in stem-cell-based clinical trials in the setting of cardiovascular diseases (CVDs).[7,8] Stem-cell derived EVs are lipid-enclosed particles containing vast protein, RNA, and lipid content; they are therefore capable of modulating diverse pathways, while importantly avoiding the risk of tumorigenicity and immunogenicity. In the context of CVD, EVs have displayed proangiogenic, immunosuppressive, and antioxidant properties; however, their antifibrotic actions remain obscure.[9,10] Notably, a

number of small animal models of myocardial infarction have cited reduced infarct size with treatment.[11] Furthermore, a recent study found that EVs promoted myotube formation and reduced fibrotic nodule-size and number from myoblast and muscle fibroblast cultures, respectively.[12] The objective of the current study was to assess the effects of extracellular vesicles on diastolic function and fibrosis in a large animal model of chronic myocardial ischemia, and to assess the impact of a high fat diet on the effect.

Methods

Swine Model of High Fat Diet and Chronic Myocardial Ischemia

Animal care and procedures were conducted with veterinary staff, in accordance with protocols approved by the Institutional Animal Care and Use Committee (IACUC) of Rhode Island Hospital (Lifespan). IACUC Approval Number 017316 on 10/17/2016. The data, analytic methods, and study materials are and will continue to be available, upon request.

The swine model of metabolic syndrome and chronic myocardial ischemia have been previously described.[13,14] Briefly, forty intact male Yorkshire swine were administered either a normal diet (ND; n=17) or high fat diet (HFD; n=23) 4% cholesterol, 17.2% coconut oil, 2.3% corn oil, 1.5% sodium cholate, and 75% regular chow (Sinclair Research, Columbia, MO). This diet is a validated method of producing clinical characteristics of metabolic syndrome, such as hypertension, dyslipidemia, and impaired glucose tolerance.[15] HFD indeed presented with hypercholesterolemia, dyslipidemia, and hyperglycemia; these metabolic parameters are recorded in the previous study.[13]

At eleven weeks of age, swine underwent placement of an ameroid constrictor on the left circumflex artery (LCx). First, preoperative antibiotic prophylaxis and antiplatelet therapy was provided, followed by general anesthesia induced by intramuscular Telazol (4.4 mg/kg) and Xylazine (2.2 mg/kg). The chest was entered via a left thoracotomy, and the LCx was identified and dissected in the left atrio-ventricular (A-V) groove. A vessel loop was placed around the artery and occluded for two minutes. After LCx occlusion, 5 ml of gold microspheres (BioPal, Worcester, MA) were injected into the left atrial appendage, and an ameroid constrictor (Research Instruments SW, Escondido CA) of appropriate size, as determined by the surgical team, was placed around the LCx. One ml of nitroglycerin solution (Baxter International, Deerfield, IL) was administered topically to the LCx to prevent spasm, and amiodarone (5 mg/kg) was given intravenously as needed to prevent arrhythmias.

EV Isolation and Injection

Human bone marrow-derived mesenchymal stem cells (Lonza PT-2501; Allendale, NJ) were cultured in growth medium (High-glucose DMEM (Gibco 11965084; Waltham, MA), supplemented with 10% Fetal Bovine Serum (Sigma Aldrich F0926; St. Louis, MO), and 1% Penicillin/Streptomycin (Gibco 15140122; Waltham, MA). Cells were grown to 80–90% confluency, at which point growth medium was replaced with serum-free RPMI media (ThermoFisher 11875; Waltham, MA) for 24 hours. Extracellular vesicles were isolated by ultracentrifugation at 100,000 g for 70 min., washed with sterile phosphate-buffered saline

(PBS), and ultra-centrifuged again at 100,000 g for 70 min. The pellet was re-suspended in 10% Dimethyl Sulfoxide (DMSO) in PBS. Protein was quantified using a commercial radio-immunoprecipitation assay (Pierce™ BCA Protein Assay Kit, ThermoFisher Scientific, Waltham, MA).

Two weeks following ameroid placement, ND and HFD swine were subdivided into control and treatment groups. All animals received preoperative antibiotics, anesthesia, and preparation similar to that of the ameroid placement procedure. A 2 to 3 cm incision was made below the initial thoracotomy. The left atrioventricular groove was accessed and the ameroid constrictor was visualized around the LCx, at which point 50 μg of EVs suspended in 2 ml of normal isotonic saline or 2 ml of isotonic saline were injected intramyocardially at 8 distinct sites throughout the ischemic territory. The incision was then closed in layers after hemostasis.

Terminal Harvest Procedure and Hemodynamic Measurements

Five weeks post-EV treatment, animals were sacrificed in a terminal harvest procedure, as previously described.[13] Briefly, following general anesthesia, a pressure monitor catheter was advanced from the femoral artery into the ascending artery in a retrograde fashion. The chest was entered via a median sternotomy, where 5 ml of Luteum and 5 ml of Europium-labeled microspheres were injected into the left atrium; during injections, 10 ml of blood was drawn from the femoral catheter. This procedure was repeated with 5 ml of Samarium-labeled microspheres and atrial pacing at 150 beats per minute. Next, a 6F catheter sheath was introduced into the apex of the left ventricle to insert a pressure-volume monitoring catheter (Millar).

Multiple hemodynamic measurements of the left ventricle have been previously reported, and the current study evaluated end diastolic pressure volume relationship (EDPVR) through assessment of multiple indices of hemodynamic performance and extrapolation of pressure-volume loops. Following recording of hemodynamic parameters, animals were euthanized by exsanguination and heart excision. The left ventricular tissue was obtained and divided into 16 pieces according to the distribution of the LCx and left anterior descending (LAD) coronary arteries. The tissue specimens were either placed in 10% formalin solution for histology or flash frozen in liquid nitrogen for protein expression.

Histology

Five μm thick, frozen tissue sections were prepared and mounted on slides for PicroSirius red or Von Kossa staining. For Picrosirius red staining – sirius red solution was used to cover the tissue section and incubated for 10 min., then dehydrated in gradient alcohol, and subsequently cleared in xylene and coverslipped. For Von Kossa staining – tissue sections were covered with 5% silver nitrate solution for 60 min. with exposure to ultraviolet light, then rinsed with several changes of distilled water. Slides were then incubated in 5% sodium thiosulfate solution for 3 min, and rinsed for 2 min with running tap water followed by 2 changes of distilled water. Next, slides were counterstained with hematoxylin and eosin.[16] Brightfield composite images were acquired per specimen with a Panoramic Midi (3D HISTECH Ltd.; Budapest, Hungary) digital slide scanner to 40x magnification.

Image processing was performed on QuPath software (University of Edinburgh; Edinburgh, Scotland), where five interstitial and perivascular areas were selected at 10x and 20x magnification respectively for Sirius Red, and five areas of 10x magnification for Von Kossa. Images were then transferred to ImageJ (National Institutes of Health; Bethesda, MD) for analysis by color thresholding or measurement of cardiomyocyte diameter.[17,18]

Immunofluorescence

Five-μm thick, frozen tissue sections were washed with PBS (3 × 5 min). Pepsin treatment was applied and slides were baked for 30 min at 37°C oven, then washed with PBS (3 × 5 min.) Sections were then covered with bovine serum albumin (BSA) for 20 min at room temperature then removed, at which point primary antibody Vimentin (Thermo Fisher Scientific, PA1–10003; Waltham, MA) at 1:2000 dilution in PBS and α smooth muscle actin (αSMA) at 1:200 was applied overnight at 4°C. Secondary antibodies anti-chicken, alexa fluor plus 647 (Thermo Fisher Scientific A32933; Waltham, MA) and anti-rabbit, CY3 (Thermo Fisher Scientific A10520; Waltham, MA) were added at 1:2000 dilution in PBS for 40 min at room temperature. Slides were washed, stained with DAPI for 10 min at 1:500, then washed again. Slides were placed on a Sudan black block for 5 min, washed with running water for 20 min, then coverslipped with resin. Composite images were acquired per sample with a Panoramic Midi (3D HISTECH Ltd.; Budapest, Hungary) digital slide scanner to 40x magnification. Image processing was performed on CaseViewer software (3DHISTECH Ltd.; Budapest, Hungary), where five images were acquired per sample at 10x magnification and transferred to ImageJ (National Institutes of Health; Bethesda, MD) for analysis.

Western Blotting

Ischemic left ventricular tissue was collected, flash-frozen, and later homogenized to prepare protein lysates. Protein concentration was determined using a radioimmunoprecipitation assay (Thermo Fisher Scientific; Waltham, MA). Whole-tissue lysates were then fractionated onto 4% to 12% Bis-Tris Gel (Thermo Fisher Scientific; Waltham, MA) and transferred onto nitrocellulose or PVDF membranes (BioRad Laboratories Inc.; Hercules, CA. Blocking buffer was applied for 1 hour, followed by incubation with primary antibodies overnight at 4°C; primary antibodies were added at 1:1,000 dilution, and were from Cell Signaling (Danvers, MA), Novus Biologicals (Littleton, CO), and Abcam (Cambridge, MA). Loading error was corrected with anti-GAPDH or anti-α-tubulin. The secondary antibodies anti-rabbit and anti-mouse (Cell Signaling; Danvers, MA) were added at 1:10,000 dilution for 1 hour at room temperature. Images were visualized using chemiluminescence (G-box; Syngene; Cambridge, England). Band densitometry was determined with ImageLab software (BioRad Laboratories Inc.; Hercules, CA) and normalized.

Statistical Analysis

All data were analyzed using GraphPad Prism 7.04 (GraphPad Software Inc.; San Diego, CA) using two-way ANOVA. Post hoc analysis was performed by the Bonferroni multiple comparison test. Results are reported as mean and SEM with respective p-values for each group (ND-C, ND-EV, HFD-C, and HFD-EV).

Results

Myocardial Function and Collagen Deposition

End diastolic pressure volume relationship (EDPVR), measured by the slope of the pressure-volume curve when the left ventricle is filled and interpreted as ventricular stiffness, was significantly reduced by EV treatment (p=0.002) (Figure 1). Histological assessment of the ischemic myocardial territory found a significant improvement in perivascular collagen density with EV treatment (p=0.032) (Figure 2A). Interstitial collagen was unaffected by EVs (Figure 2B). Similarly Collagen I and collagen III expression levels were unchanged by diet or treatment; however, EVs appeared to be associated with a trend in increasing collagen III in both diet cohorts and reducing the ratio of collagen I to collagen III in the ischemic territory of each animal. (Figure 2D–F).

Extracellular Matrix Remodeling

Interestingly, intermediate filament vimentin, a marker of fibroblasts and cardiac stem cells, was associated with a significant interaction between diet and EV-treatment (p=0.044) (Figure 3A,C)); specifically, ND-EV compared to ND-C trended upward; whereas HFD-EV trended downward compared to a relatively high level of the marker in HFD-C. A measure of the fraction of myofibroblasts, by the ratio of α smooth muscle actin (αSMA) and vimentin overlap to total vimentin, also had a significant although slight interaction (p=0.049) (Figure 3B–C). ND-C, ND-EV, and HFD-C animals shared a similar fraction, while HFD-C maintained a high baseline in the fraction of myofibroblasts to total vimentin. Extracellular matrix remodeling factor lysyl oxidase (LOX) was not affected by diet nor treatment, while matrix metalloproteinase 13 (MMP-13) was significantly reduced in the HFD group (p=0.012) (Figure 3D–E).

Mineralization and Muscle Histology

Indirect examination of calcium deposition with silver nitrate solution saw a significant reduction in calcium minerals with EV treatment (p=0.0264) (Figure 4A). It is important to note, that the Von Kossa staining procedure described in the methods section is a measure of extracellular and intracellular calcium salts. Osteopontin, a structural and regulatory component of mineralized extracellular matrices, was upregulated with EV-treatment (p=0.0046) (Figure 4B).

Muscle fiber area, measured by picrosirius red staining, was observed to be significantly reduced in HFD compared to ND groups (p=0.0259) (Figure 2C). At the cellular level, extracellular vesicles reduced cardiomyocyte diameter (p<0.0001), which was also significantly different between diets (p=0.0005) (Figure 4C). Thick filament, cardiac myosin, was not significant but trended upward with EV-treatment across both diets (Figure 4D).

Inflammation and Oxidative Stress

An examination of inflammation and oxidative stress-related signaling in the groups found a significant downregulation of tumor necrosis factor α (TNFα) in HFD swine (p= 0.0002) (Figure 5A). A similar pattern was observed with superoxide producers NADPH oxidase 2

(NOX2) (p=0.0036) and NOX4 (p=0.008) (Figure 5B–C). The antioxidant catalase (CAT) was not associated with any changes (Figure 5D). Mitochondrial antioxidant superoxide dismutase 1 (SOD1) was significantly reduced in HFD (p=0.034), while SOD2 was insignificant (Figure 5E–F).

Molecular Signaling Pathways

Phosphorylated AMP-activated protein kinase (pAMPK) and its total form were insignificant across diets and treatment; although the ratio of phosphorylated to total AMPK notably trended downwards with EV treatment in both diet cohorts (Figure 6A–C). The expression of mechanistic target of rapamycin (mTOR) was upregulated with EV-treatment (p=0.0208) (Figure 6D). Phosphorylated glycogen synthase kinase 3β at residue serine 9, which results in its inhibition, was reduced in the HFD group (p=0.020) (Figure 6E). Diet and/or EV treatment did not significantly effect mitochondrial- and metabolic-related factors, PPARG coactivator 1α (PGC1α) nor sirtuin 1 (SIRT1), respectively. Receptors of angiotensin II (AngII), angiotensin II receptor type 1 (AT1R) and type 2 (AT2R), were also unaffected by diet or treatment.

Discussion

This study reports a significant reduction in EDPVR with EV-therapy in both normal and high fat diet groups in a chronically ischemic myocardial model, which was associated with reductions in perivascular collagen density, calcium mineralization, and cardiomyocyte hypertrophy (Graphical Abstract). These functional and histological measures reflect that EV treatment ameliorated impaired relaxation associated with chronic ischemia across both dietary cohorts, due to EV-mediated improvements in the myocardium’s substructure.

Hypoxic injury secondary to ischemia results in extensive cardiomyocyte apoptosis and necrosis that compromise the structural integrity of the myocardium, and result in compensatory cardiomyocyte hypertrophy and collagen deposition. We did not in fact find an increase in muscle fiber density with EVs; however, we observed a significant reduction in cardiomyocyte hypertrophy across both diets in accordance with an increased trend in β-cardiac myosin that is consistent with improvement in contractility and systolic function found in our previous study.[13] We further encourage the evaluation of cardiac myosin-binding protein-C which has been found as an integral regulator in cross-bridge cycling, particularly favoring detachment and hence relaxation.[19] Nonetheless, EVs did not alter remodeling by interstitial or reparative fibrosis, which is now generally accepted as an important component in maintaining myocardial structure following cardiomyocyte loss.[2] Mechanical and hemodynamic stress are followed by neurohormonal changes that altogether contribute to the pathogenesis of perivascular fibrosis, stimulating the deposition of fibrous scar tissue surrounding the coronary vasculature. This process, known as reactive fibrosis impedes tissue oxygenation and promotes excessive scarring which significantly diminishes ventricular elasticity. The reduction in perivascular fibrosis combined with a notable downward trend of collagen I to collagen III seen in the EV treated cohort support a role of EVs in reducing stiffness of the metabolically stressed ischemic myocardium.

Collagen and extracellular matrix remodeling is an integral aspect of myocardial fibrosis and is stimulated by the secretion of proteolytic enzymes following the activation of fibroblasts into a myofibroblast phenotype. Interestingly, we report an interactive effect between diet and EVs in regards to fibroblast and myofibroblast markers. Vimentin is a common marker for fibroblasts, and has additionally been shown to be a marker of cardiac stem cell populations and other mesenchymal cell lineages.[20] We, therefore, speculate that the increase in total vimentin but not fraction of activated fibroblasts in ND-EV compared to control may represent increased stem cell recruitment to the myocardium for cardiac regeneration. Ibrahim *et al.* indeed found increased tissue preservation and viable mass of the heart when treated with cardiosphere-derived EVs.[21] On the other hand, HFD-EV displayed lower vimentin and myofibroblast markers relative to HFD-C, suggesting that EVs were able to inhibit adverse remodeling with HFD. This interactive finding may support EV-mediated improvements in diastolic function by different mechanisms between diets that are context-dependent. We note no changes with EVs in collagen cross-linking as assessed by LOX nor MMP-13 expression. As an array of MMPs, tissue inhibitors of matrix metalloproteinases (TIMPs), and components of the plasminogen system all play major roles in remodeling, future proteomic characterization will provide greater insight due to the sheer number of factors and value of their relative abundance.

An additional consequence attributed to loss of viable tissue is dystrophic calcification whereby calcium deposits in the setting of normal serum calcium levels, further contributing to stiffness and diastolic dysfunction. An entirely separate process, often termed calcium handling, describes the intricate homeostatic control of calcium ions within cells that is dysregulated in the ischemic heart and results in excess cytoplasmic calcium ions. Calcium ion overload has been shown to impair excitation-contraction coupling, and promote cellular hypertrophy and eventually necrosis.[22–24] Calcium mineral content, as measured by Von Kossa staining which indirectly measures for intra- and extracellular calcium salts, showed reduced ischemic myocardial calcium levels with EV treatment. Whether EVs mediated intra- or extracellular calcium is out of the scope of the current study; however, we perhaps relatedly observed that EVs upregulated osteopontin protein expression; a calcium-binding phosphoprotein abundant in bone, but overexpressed at sites of tissue injury.[25,26] An elegant study by Steitz *et al.* revealed osteopontin as an inhibitor of ectopic calcification.[27] Separately, EVs were associated with reduced cardiomyocyte hypertrophy, which may be linked to mediation of calcium ion homeostasis.[23]

Transitioning to underlying, neurohormonal signaling related to the renin-angiotensin aldosterone system (RAAS), the pro-and anti-fibrotic angiotensin II receptors, AT1R and AT2R respectively, revealed no effects by diet nor EVs. Although, RAAS is commonly intertwined with heart failure, the study used Yorkshire swine that were young and healthy prior to induction of chronic ischemia which was relatively transient and did not comprise the scope of pathological elements seen in patients with long standing disease. As a result, changes in RAAS in our porcine model may not be as apparent compared to natural multifactorial disease progression in the setting of multiple comorbidities which usually involves RAAS activation early on.

We proceeded to examine the effects related to diet and EVs on metabolic signaling, which revealed a significant increase in mTORC1 with EVs, consistent with a downward trend in its inhibitor and energy sensor, AMPK. Quite interestingly, this trend in reduced pAMPK to its total form suggests an increased energy supply with EVs. mTORC1 is a regulator of protein synthesis, cell proliferation, metabolism, and autophagy; furthermore, it has been shown to be associated with both adaptive and maladaptive cardioprotection in disease models.[28] Downstream targets of mTORC1 relating to mitochondrial biogenesis and metabolism, PGC1α and pGSK3β respectively, were unaffected by EVs. Although the study's downstream findings relating to mTORC1 are negative, this master regulator mediates a variety of pathways and we speculate that it may contribute to improved diastolic function through increased protein synthesis and inhibition of autophagy.[29] EVs were not associated with any changes in selected inflammatory and oxidative stress signaling; although the previous study by our lab found reduced oxidative stress with treatment.[13] Thus, the underlying signaling related to redox control in our model remains obscure.

The nature of our model importantly allowed an examination of the impact of diet. Comorbidities are widely prevalent risk factors for the onset and progression of cardiovascular disease due to underlying changes in the metabolic and inflammatory molecular landscape that result in adverse changes at the cellular and functional levels.[30] Previous studies by our lab indeed found differential functional, angiogenic, and signaling outcomes between ND and HFD swine with EV treatment – particularly an impaired angiogenic capacity, paradoxical angiogenic signaling and disparate global gene expression.[13,14] The current study provides further histological insight where HFD was associated with substantial muscle fiber loss and compensatory cardiomyocyte hypertrophy. In addition, significant reductions in TNFα, NOX2, NOX4, SOD1, pGSK3β, and MMP13 expression in the ischemic myocardium were observed.

MMP13 is a collagenase that cleaves collagens I, II, and III among other ECM factors, and has been linked to atheromatous rather than fibrous plaques. Despite considerable hypercholesterolemia in the HFD-C, MMP-13 was interestingly downregulated perhaps suggesting stable lesions, an adaptive phenomenon, or even impaired wound healing.[31] We, in addition, found decreased TNFα, NOX2, and NOX4 which may suggest reduced proinflammatory response that inhibits superoxide production by NOX enzymes. However, we note a hallmark study that showed short-term NOX-derived ROS as essential for vasculoprotection.[32] The reduction in SOD1, without any changes in SOD2 nor catalase, may simply be explained by downregulation of pro-oxidative enzymes such as NOX. We further report a reduction in the phosphorylated or inhibited form of GSK3β in the HFD group; this protein has been implicated in the anti-hypertrophic response and cardiovascular development.[33] However, a previous study by our lab found that inhibition of GSK3β improved myocardial angiogenesis and perfusion in a porcine model of chronic myocardial ischemia with metabolic syndrome.[34] This may point towards quite different effects of GSK3β in nonmetabolic and metabolic syndrome.

Importantly, despite the molecular disparities between HFD and ND that have been highlighted, EV therapy was able to improve the extracellular matrix, cell structures, and ultimately diastolic function across both diets. This consistency in outcomes across diets

is particularly relevant for the future translation of EVs to the clinic, where coexisting risk factors are prevalent and contribute to diastolic dysfunction. Currently, no curative treatment options exist for HFpEF that specifically target relaxation without interfering with contractility. EVs, therefore, hold the potential to reverse the underlying process of perivascular collagen deposition which to our knowledge is unprecedented. This study further provides the impetus for future investigation with both positive and negative findings presented relating to molecular signaling, which will be valuable in future translation and perhaps optimization via bioengineering of EVs for further precision.

Supplementary Material

Refer to Web version on PubMed Central for supplementary material.

Acknowledgements:

We would like to thank Founder of iHisto (Woburn, MA), Kelven Wong, for histological service and support. We further acknowledge that the graphical abstract was created with BioRender.com.

Sources of Funding Statement:

Funding for this research was provided by the National Heart, Lung, and Blood Institute (NHLBI) [R01HL46716; R01HL128831–01A1; P20 GM103652 (FWS)]; NHLBI 1R01HL133624 (MRA).

Biographies

Glossary of Abbreviations

ECM	extracellular matrix
HFpEF	heart failure with preserved ejection fraction
CVD	cardiovascular disease
EV	extracellular vesicle
LCx	left circumflex artery
A-V	atrio-ventricular
LAD	left anterior descending

EDPVR	end diastolic pressure volume relationship
COL1A1	collagen I type 1
COL3A1	collagen III type 1
LOX	lysyl oxidase
MMP-13	matrix metalloproteinase 13
SPP1	osteopontin
β-MHC	heavy chain cardiac myosin
αSMA	α smooth muscle actin
TNFα	tumor necrosis factor α
NOX2/4	NADPH oxidase 2/4
SOD1/2	superoxide dismutase 1/2
AMPK	AMPK-activated protein kinase
mTORC1	mechanistic target of rapamycin complex1
GSK3β	glycogen synthase kinase 3 β
PGC1α	PPARG coactivator 1α
SIRT1	sirtuin 1
AT1R	angiotensin II receptor type 1
AT2R	angiotensin II receptor type 2.
GAPDH	glyceraldehyde phosphate dehydrogenase
AngII	angiotensin II
SV	stroke volume
CO	cardiac output
ESPVR	end systolic pressure volume relationship
dp/dt	derivative of pressure over time
Tau	left ventricular diastolic time constant
CAII	carbonic-anhydrase
TIMPs	tissue inhibitors of matrix metalloproteinases
RAAS	renin-angiotensin-aldosterone system

References

1. Roth GA, Johnson C, Abajobir A, et al. Global, Regional, and National Burden of Cardiovascular Diseases for 10 Causes, 1990 to 2015. J Am Coll Cardiol. 2017;70(1):1–25. doi:10.1016/j.jacc.2017.04.052 [PubMed: 28527533]
2. González A, Schelbert EB, Díez J, Butler J. Myocardial Interstitial Fibrosis in Heart Failure: Biological and Translational Perspectives. J Am Coll Cardiol. 2018;71(15):1696–1706. doi:10.1016/j.jacc.2018.02.021 [PubMed: 29650126]
3. Similarities Komamura K. and Differences between the Pathogenesis and Pathophysiology of Diastolic and Systolic Heart Failure. Cardiol Res Pract. 2013;2013:824135. doi:10.1155/2013/824135 [PubMed: 24459600]
4. Cavalera M, Wang J, Frangogiannis NG. Obesity, metabolic dysfunction, and cardiac fibrosis: pathophysiological pathways, molecular mechanisms, and therapeutic opportunities. Transl Res. 2014;164(4):323–335. doi:10.1016/j.trsl.2014.05.001 [PubMed: 24880146]
5. Kuznetsova T, Herbots L, López B, et al. Prevalence of left ventricular diastolic dysfunction in a general population. Circ Heart Fail. 2009;2(2):105–112. doi:10.1161/CIRCHEARTFAILURE.108.822627 [PubMed: 19808325]
6. Mandinov L, Eberli FR, Seiler C, Hess OM. Diastolic heart failure. Cardiovasc Res. 2000;45(4):813–825. doi:10.1016/S0008-6363(99)00399-5 [PubMed: 10728407]
7. Meyer GP, Wollert KC, Lotz J, et al. Intracoronary bone marrow cell transfer after myocardial infarction: eighteen months' follow-up data from the randomized, controlled BOOST (BOne marrOw transfer to enhance ST-elevation infarct regeneration) trial. Circulation. 2006;113(10):1287–1294. doi:10.1161/CIRCULATIONAHA.105.575118 [PubMed: 16520413]
8. Bartunek J, Terzic A, Davison BA, et al. Cardiopoietic cell therapy for advanced ischaemic heart failure: Results at 39 weeks of the prospective, randomized, double blind, sham-controlled CHART-1 clinical trial. Eur Heart J. 2017;38(9):648–660. doi:10.1093/eurheartj/ehw543 [PubMed: 28025189]
9. Davidson SM, Yellon DM. Exosomes and cardioprotection - A critical analysis. Mol Aspects Med. 2018;60:104–114. doi:10.1016/j.mam.2017.11.004 [PubMed: 29122678]
10. Karbasiafshar C, Sellke FW, Abid MR. Mesenchymal stem cell-derived extracellular vesicles in the failing heart: past, present, and future. Am J Physiol Circ Physiol. 2021;320(5):H1999–H2010. doi:10.1152/ajpheart.00951.2020
11. Alibhai FJ, Tobin SW, Yeganeh A, Weisel RD, Li RK. Emerging roles of extracellular vesicles in cardiac repair and rejuvenation. Am J Physiol - Hear Circ Physiol. 2018;315(4):H733–H744. doi:10.1152/ajpheart.00100.2018
12. Novokreshchenova AN, Butorina NN, Payushina OV, Sheveleva ON, Evtushenko EG, Domaratskaya EI. Mesenchymal Stromal Cell-Derived Extracellular Vesicles: Their Features and Impact on Fibrosis and Myogenesis in Vitro. Biochem (Moscow), Suppl Ser A Membr Cell Biol. 2020;14(4):289–297. doi:10.1134/S1990747820100013
13. Aboulgheit A, Potz BA, Scrimgeour LA, et al. Effects of High Fat Versus Normal Diet on Extracellular Vesicle-Induced Angiogenesis in a Swine Model of Chronic Myocardial Ischemia. J Am Heart Assoc. 2021;10(4):e017437. doi:10.1161/JAHA.120.017437 [PubMed: 33559477]
14. Scrimgeour LA, Potz BA, Aboul Gheit A, et al. Extracellular Vesicles Promote Arteriogenesis in Chronically Ischemic Myocardium in the Setting of Metabolic Syndrome. J Am Heart Assoc. 2019;8(15):1–14. doi:10.1161/jaha.119.012617
15. Zhang X, Lerman LO. Investigating the Metabolic Syndrome: Contributions of Swine Models. Toxicol Pathol. 2016;44(3):358–366. doi:10.1177/0192623316630835 [PubMed: 26933085]
16. Fischer AH, Jacobson KA, Rose J, Zeller R. Hematoxylin and eosin staining of tissue and cell sections. CSH Protoc. 2008;2008:pdb.prot4986. doi:10.1101/pdb.prot4986
17. Bankhead P, Loughrey MB, Fernández JA, et al. QuPath: Open source software for digital pathology image analysis. Sci Rep. 2017;7(1):16878. doi:10.1038/s41598-017-17204-5 [PubMed: 29203879]
18. Schneider CA, Rasband WS, Eliceiri KW. NIH Image to ImageJ: 25 years of image analysis. Nat Methods. 2012;9(7):671–675. doi:10.1038/nmeth.2089 [PubMed: 22930834]

19. Tong CW, Nair NA, Doersch KM, Liu Y, Rosas PC. Cardiac myosin-binding protein-C is a critical mediator of diastolic function. Pflugers Arch. 2014;466(3):451–457. doi:10.1007/s00424-014-1442-1 [PubMed: 24442121]
20. Klopsch C, Gaebel R, Lemcke H, et al. Vimentin-Induced Cardiac Mesenchymal Stem Cells Proliferate in the Acute Ischemic Myocardium. Cells Tissues Organs. 2018;206(1–2):35–45. doi:10.1159/000495527 [PubMed: 30630170]
21. Ibrahim AG-E, Cheng K, Marbán E. Exosomes as Critical Agents of Cardiac Regeneration Triggered by Cell Therapy. Stem Cell Reports. 2014;2(5):606–619. doi:10.1016/j.stemcr.2014.04.006 [PubMed: 24936449]
22. ED A, CJ L, Kornél K, TA. W Calcium and Excitation-Contraction Coupling in the Heart. Circ Res. 2017;121(2):181–195. doi:10.1161/CIRCRESAHA.117.310230 [PubMed: 28684623]
23. Molkentin JD, Lu J-R, Antos CL, et al. A Calcineurin-Dependent Transcriptional Pathway for Cardiac Hypertrophy. Cell. 1998;93(2):215–228. doi:10.1016/S0092-8674(00)81573-1 [PubMed: 9568714]
24. Nakayama H, Chen X, Baines CP, et al. Ca2+- and mitochondrial-dependent cardiomyocyte necrosis as a primary mediator of heart failure. J Clin Invest. 2007;117(9):2431–2444. doi:10.1172/JCI31060 [PubMed: 17694179]
25. Liaw L, Birk DE, Ballas CB, Whitsitt JS, Davidson JM, Hogan BL. Altered wound healing in mice lacking a functional osteopontin gene (spp1). J Clin Invest. 1998;101(7):1468–1478. doi:10.1172/JCI2131
26. O'Brien ER, Garvin MR, Stewart DK, et al. Osteopontin is synthesized by macrophage, smooth muscle, and endothelial cells in primary and restenotic human coronary atherosclerotic plaques. Arterioscler Thromb a J Vasc Biol. 1994;14(10):1648–1656. doi:10.1161/01.atv.14.10.1648
27. Steitz SA, Speer MY, McKee MD, et al. Osteopontin inhibits mineral deposition and promotes regression of ectopic calcification. Am J Pathol. 2002;161(6):2035–2046. doi:10.1016/S0002-9440(10)64482-3 [PubMed: 12466120]
28. Sciarretta S, Forte M, Frati G, Sadoshima J. New Insights Into the Role of mTOR Signaling in the Cardiovascular System. Circ Res. 2018;122(3):489–505. doi:10.1161/CIRCRESAHA.117.311147 [PubMed: 29420210]
29. Li Z, Wang J, Yang X. Functions of autophagy in pathological cardiac hypertrophy. Int J Biol Sci. 2015;11(6):672–678. doi:10.7150/ijbs.11883 [PubMed: 25999790]
30. Boodhwani M, Sodha NR, Mieno S, et al. Functional, cellular, and molecular characterization of the angiogenic response to chronic myocardial ischemia in diabetes. Circulation. 2007;116(11 Suppl):I31–7. doi:10.1161/CIRCULATIONAHA.106.680157 [PubMed: 17846323]
31. SG K, Uwe S, Elena R, et al. Evidence for Increased Collagenolysis by Interstitial Collagenases-1 and −3 in Vulnerable Human Atheromatous Plaques. Circulation. 1999;99(19):2503–2509. doi:10.1161/01.CIR.99.19.2503 [PubMed: 10330380]
32. Shafique E, Torina A, Reichert K, et al. Mitochondrial redox plays a critical role in the paradoxical effects of NAPDH oxidase-derived ROS on coronary endothelium. Cardiovasc Res. 2017;113(2):234–246. doi:10.1093/cvr/cvw249 [PubMed: 28088753]
33. Hardt SE, Sadoshima J. Glycogen synthase kinase-3beta: a novel regulator of cardiac hypertrophy and development. Circ Res. 2002;90(10):1055–1063. doi:10.1161/01.res.0000018952.70505.f1 [PubMed: 12039794]
34. Potz BA, Sabe AA, Elmadhun NY, et al. Glycogen Synthase Kinase 3β Inhibition Improves Myocardial Angiogenesis and Perfusion in a Swine Model of Metabolic Syndrome. J Am Heart Assoc. 2016;5(7):e003694. doi:10.1161/JAHA.116.003694 [PubMed: 27405812]

Perspective Statement

Cardiovascular disease is the leading cause of death globally, which is further exacerbated by the prevalence of comorbidities and thus requires the investigation of novel therapeutic modalities. In a large animal model of chronic myocardial ischemia, extracellular vesicles improved diastolic function, and reduced perivascular fibrosis, mineralization and hypertrophy in normal and high fat diet swine.

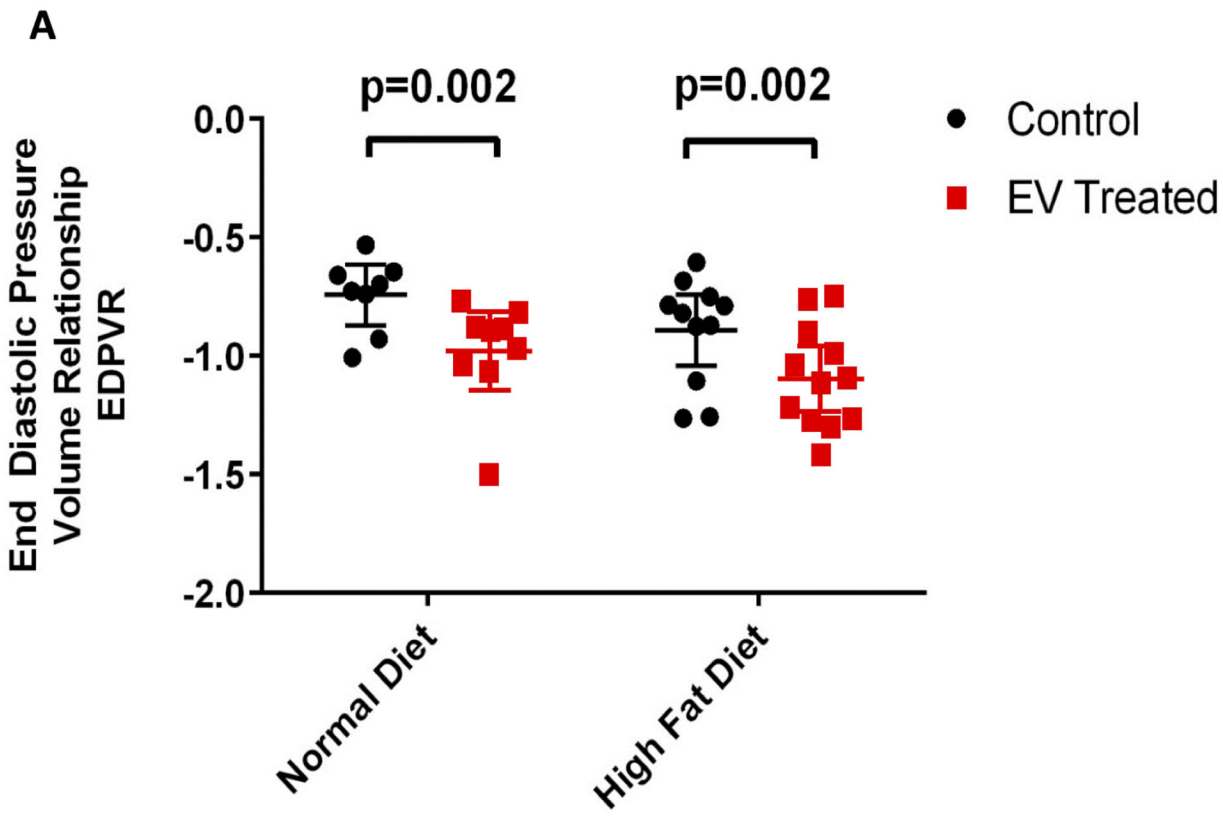

Figure 1: Extracellular Vesicles Improved Diastolic Function.

Quantification of end diastolic function pressure volume relationship (EDPVR) as a measure of diastolic performance. The analysis was performed by assessment of multiple indices of hemodynamic performance and extrapolation of pressure-volume loops. Data is graphed as mean with SEM, with main effect of diet as large bracket and main effect of EVs as inner brackets.

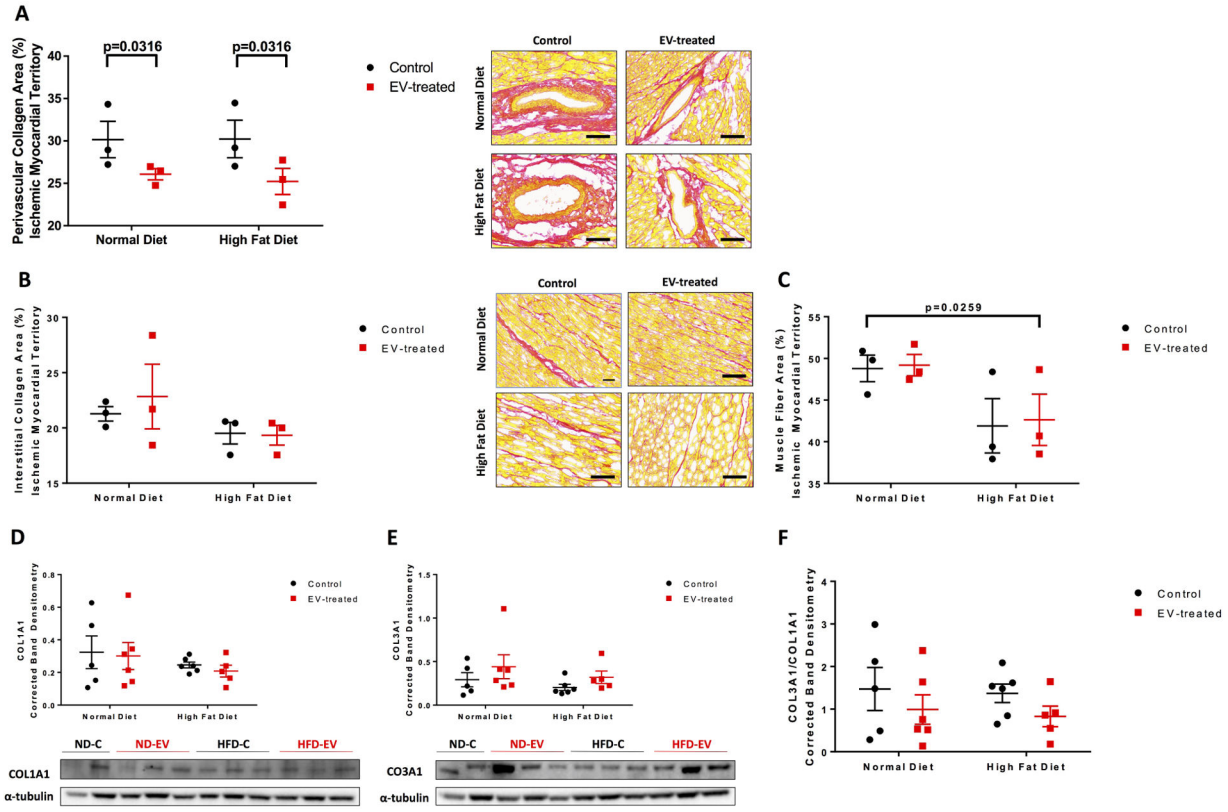

Figure 2: Perivascular fibrosis reduced with EV-treatment.

The ischemic myocardial territory was examined for (A) perivascular collagen, (B) interstitial collagen, and (C) muscle fiber areas by Picrosirius Red staining technique. Five areas at 10x magnification per animal were measured and analyzed by 2-way ANOVA. Western blots of protein lysates from porcine ischemic myocardial tissue were performed as indicated with quantitative analyses normalized to α-tubulin and representative images (D) COL1A1 and (E) COL3A1. (F) Ratio of COL3A1 to COL1A1. Data is graphed as mean with SEM. COL1A1, collagen I type 1; COL3A1, collagen III type 1.

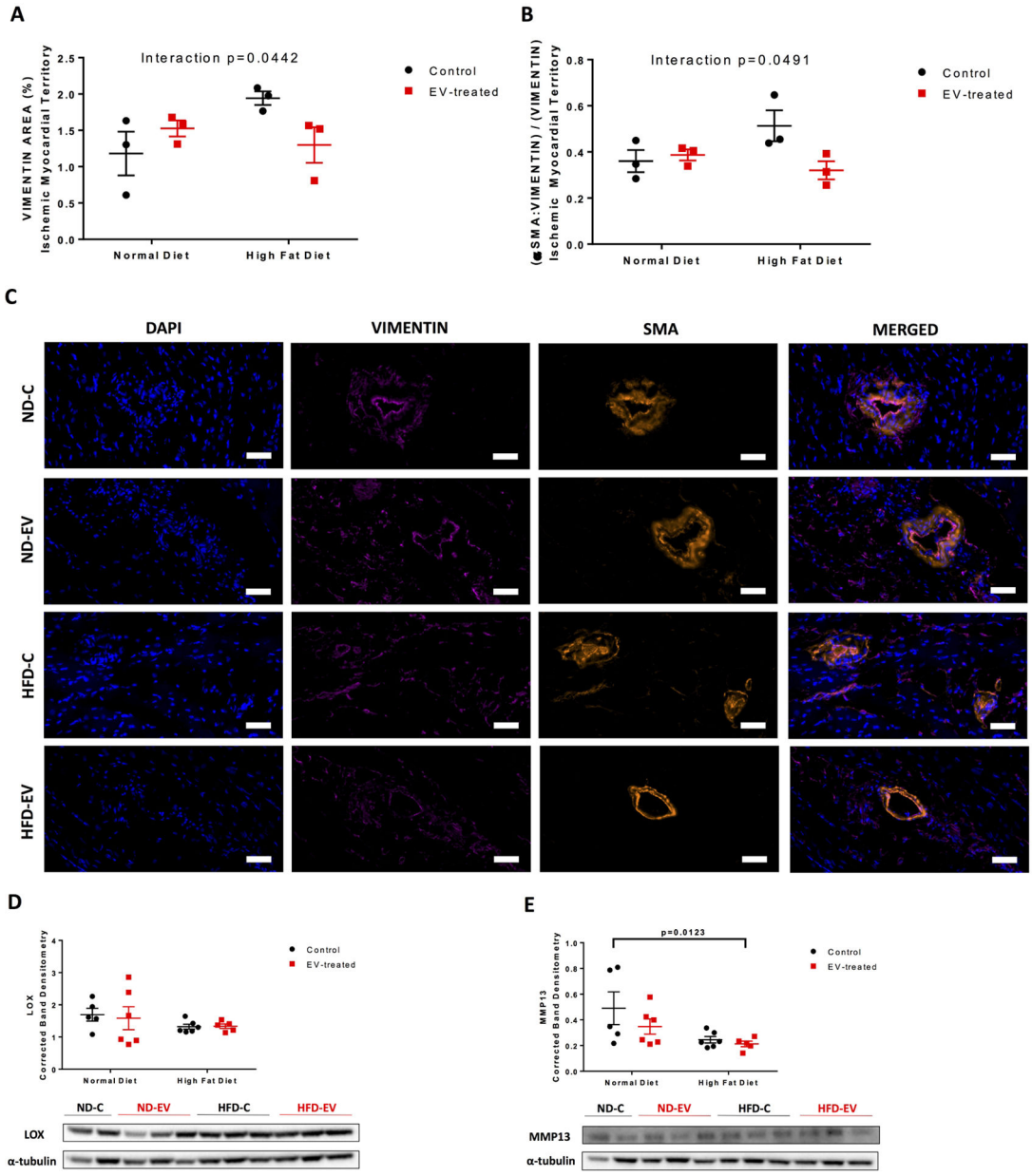

Figure 3: Interaction between EVs and Diet with Markers of Fibroblasts and Myofibroblasts.

Cardiac fibroblast and stem-cell marker (A) vimentin percent area was measured. The fraction of myofibroblasts was measured as the (B) fraction of αSMA and vimentin positive area over total vimentin area. Analysis was performed at 10x magnification with five areas per animal. Representative images are at 40x; scale bar 50 μm. (C) and (D) Western blots of protein lysates from porcine ischemic myocardial tissue were performed as indicated with quantitative analyses normalized to α-tubulin and representative images (D) LOX and (E) MMP13. Data is graphed as mean with SEM, with main effect of diet as large bracket and main effect of EVs as inner brackets. LOX, lysyl oxidase; MMP-13, matrix metalloproteinase 13. Scale bar 100 μm.

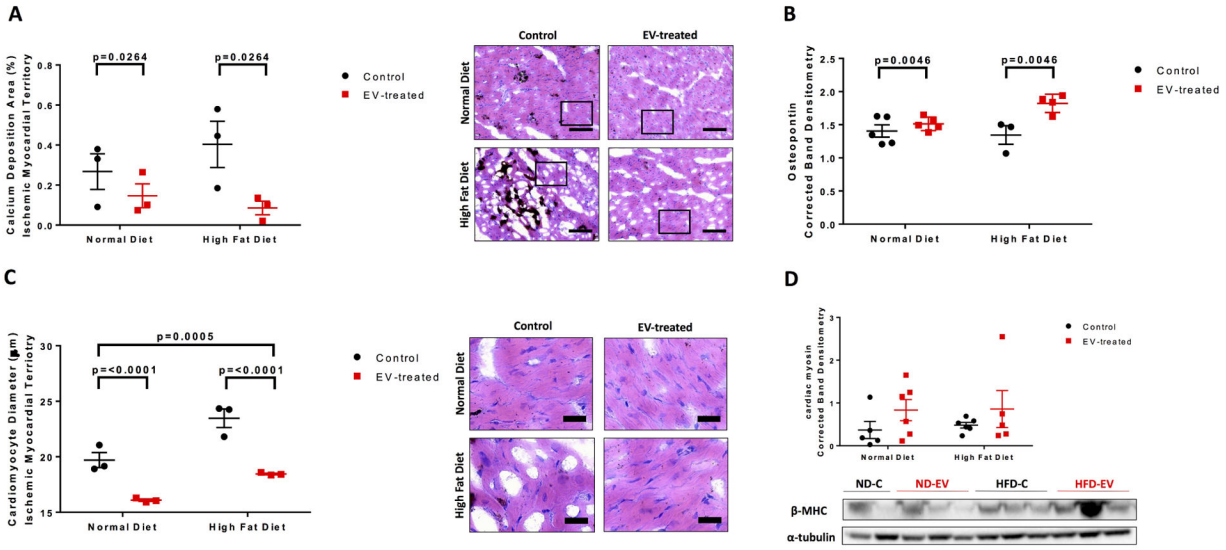

Figure 4: EV-treatment reduced calcium mineralization and cardiomyocyte hypertrophy.

Von Kossa counterstained with hematoxylin and eosin were used to measure (C) calcium deposition and (D) cardiomyocyte diameter. Five areas at 10x magnification per animal were measured and analyzed by 2-way ANOVA. Western blots of protein lysates from porcine ischemic myocardial tissue were performed as indicated with quantitative analyses normalized to α-tubulin and representative images (B) Osteopontin and (D) cardiac myosin. Blot for (B) is provided in supplementary Figure S1. Data is graphed as mean with SEM, with main effect of diet as large bracket and main effect of EVs as inner brackets. SPP1, osteopontin; β-MHC, heavy chain cardiac myosin. Scale bar are as follows (A) 100 μm and (B) 25 μm.

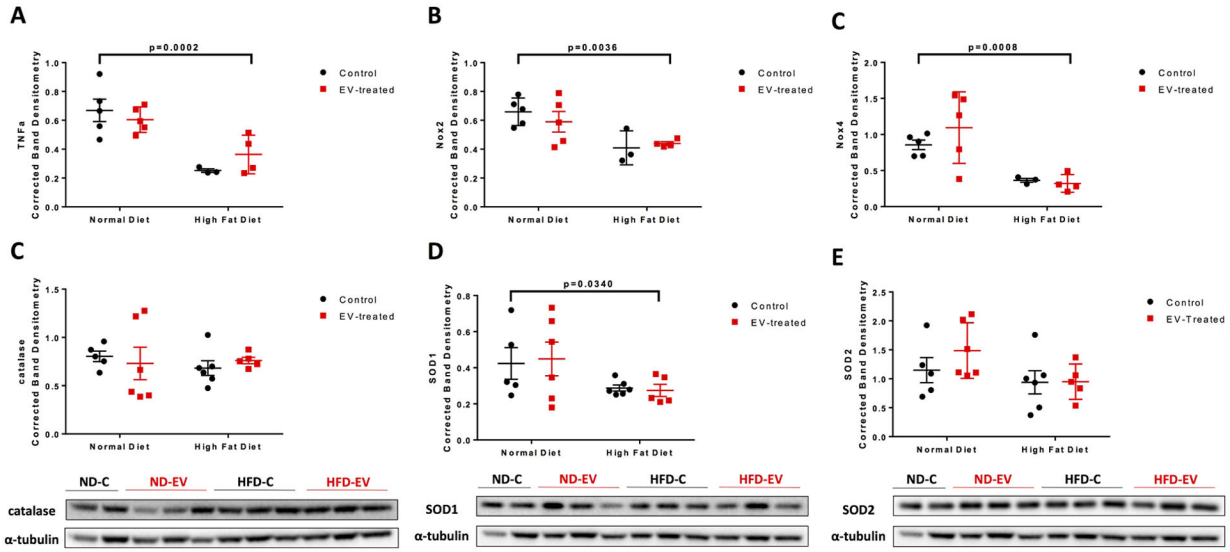

Figure 5: Inflammatory and Redox Molecular Signaling Altered by Diet.

Western blots of protein lysates from porcine ischemic myocardial tissue were performed as indicated with quantitative analyses normalized to α-tubulin and representative images (A) TNFα, (B) NOX2, (C) NOX4, (D) catalase, (E) SOD1, (F) SOD2. Blots for (A), (B), and (C) are provided in supplementary Figure S1. Data is graphed as mean with SEM, with main effect of diet as large bracket and main effect of EVs as inner brackets. TNFα, tumor necrosis factor α; NOX2/4, NADPH oxidase 2/4; SOD1/2, superoxide dismutase 1/2.

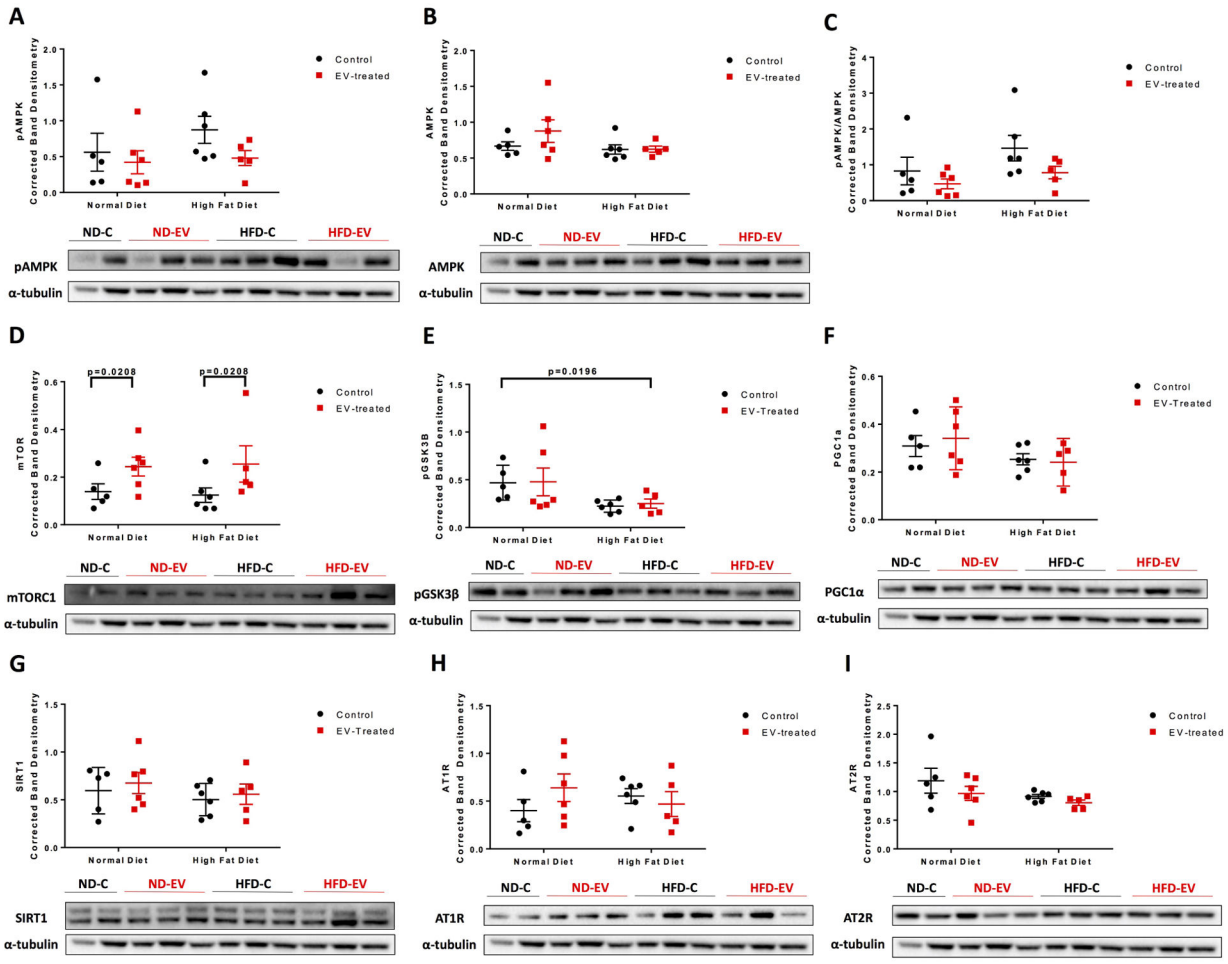

Figure 6: Molecular Signaling Pathways.

Western blots of protein lysates from porcine ischemic myocardial tissue were performed as indicated with quantitative analyses normalized to α-tubulin and representative images. Data is graphed as mean with SEM, with main effect of diet as large bracket and main effect of EVs as inner brackets. AMPK, AMPK-activated protein kinase; mTORC1, mechanistic target of rapamycin complex 1; GSK3β, glycogen synthase kinase 3 β; PGC1α, PPARG coactivator 1α; SIRT1, sirtuin 1; AT1R, angiotensin II receptor type 1; AT2R, angiotensin II receptor type.